Pergamon

Int. J. Heat Mass Transfer. Vol. 41, No. 2, pp. 323–333, 1998

Printed in Great Britain
0017–9310/98 $19.00+0.00

PII: S0017-9310(97)00132-4

Convective cool-down of a contained fluid through its maximum density temperature

HO SANG KWAK and KUNIO KUWAHARA

Space Environment Laboratory, The Institute of Space and Astronautical Science, 3-1-1 Yoshinodai, Sagamihara, Kanagawa 229, Japan

and

JAE MIN HYUN†

Department of Mechanical Engineering, Korea Advanced Institute of Science and Technology, Kusong-dong 373-1, Yusong-ku, Taejon, South Korea

(*Received* 10 *May* 1996 *and in final form* 2 *May* 1997)

Abstract—A numerical study is made of transient natural convective cool-down process of a fluid in a cylindrical container. The density–temperature relationship of the fluid is given by a quadratic function, with the maximum density ρ_m occurring at T_m. Cooling is accomplished by abruptly lowering the sidewall temperature, and the mean temperature passes through T_m in the course of cool-down. Numerical solutions are acquired to the full, time-dependent Navier–Stokes equations. The flow is governed by a properly-defined Rayleigh number Ra, the density inversion factor γ, the aspect ratio A, and the Prandtl number, Pr. Evolutions of the flow and temperature fields are analyzed. Based on the structures of the sidewall boundary layer at early times, three characteristic flow regimes are identified. The qualitative early-time behavior is determined by γ. The intermediate-stage features for large γ disclose the flow restructuring. When A or Ra is large, boundary layer waves are monitored for moderate values of γ. The analysis of time-dependent heat transfer characteristics suggests that the cool-down process is divided into several transient phases. The relevant time scales for the overall cool-down process are estimated. The specific effects of Ra, γ and A on each evolutionary stage are elaborated. © 1997 Elsevier Science Ltd.

1. INTRODUCTION

Transient buoyant convection of an initially-isothermal fluid in an enclosure, in response to the changes in thermal boundary conditions, has been widely studied. The technical issues have been mainly concerned with situations of high Rayleigh number, i.e. when the buoyancy effects are substantial. Discussions have been centered on the evolutions of convective flow pattern and temperature field, and on the relevant scales of time and boundary layer thickness. Comprehensive reviews on this subject were given by Ostrach [1] and Hyun [2].

The great majority of previous studies have been performed under the Boussinesq fluid approximation, which stipulates a linear relationship between density and temperature. However, for water and certain liquids, density cannot be described by a monotonic linear function of temperature near the melting point [3]. Instead, density ρ reaches its maximum at a specific temperature T_m, and ρ decreases when temperature deviates from T_m in both directions. The best known example is water which has maximum density at $T_m = 3.98°C$. This nonlinear behavior, termed the density inversion, brings forth a major dynamic ingredient to natural convection.

The problem has important implications in engineering applications as well. In beverage storage tanks, it is often required that the contained fluid should be maintained at a low temperature near the freezing point. Cool-down of a liquid from the initial-state high temperature to a target temperature is a crucial mission in this system. A key element is to predict the time scale for the fluid to reach a desired temperature level. These are based upon a proper understanding of the time-dependent structures of flow and temperature fields, as the system encompasses the density inversion effects during its course of cool-down.

Recently, buoyant convection of an enclosed fluid with density inversion has been studied by numerical computations and laboratory experiments [4–18]. These works revealed the prominent impacts of the density inversion in various flow configurations. Most of these studies deal with primarily steady-state situations [4–10]. A literature survey discloses that comparatively scanty attention has been given to transient natural convection with density inversion.

Robillard and Vasseur [11] investigated convective cooling of water near 4°C in a rectangular cavity with a constant cooling rate applied on all boundaries. Numerical and experimental studies on the transient natural convection of water in a sidewall-heated cavity

† Author to whom correspondence should be addressed.

NOMENCLATURE

A	aspect ratio of the cylinder, H/R
g	gravitational acceleration
H	height of the cylinder
Nu	instantaneous Nusselt number at the cylindrical sidewall, equation (12)
p	dimensionless pressure, $p = (p^* + \rho g z^*)R^2/(\rho\kappa^2 RaPr)$
p^*	pressure
Pr	Prandtl number, ν/κ
R	radius of the cylinder
r, z	dimensionless radial and vertical coordinates $(r, z) = (r^*, z^*)/R$
r^*, z^*	radial and vertical coordinates
Ra	Rayleigh number, $(\rho_m - \rho_w)gR^3/\nu\kappa\rho_m$
Ra_H	Rayleigh number based on the vertical height of the cylinder, $Ra_H \equiv RaA^3$
T	temperature
t	dimensionless time, $t = t^*(RaPr)^{1/2}\kappa/R^2$
t^*	time
u, w	dimensionless velocities in r and z directions, $(u, w) = (u^*, w^*)(RaPr)^{-1/2}R/\kappa$
u^*, w^*	velocities in r^* and z^* directions
x	horizontal coordinate scaled by 300 mm in Fig. 2
y	vertical coordinate scaled by 150 mm in Fig. 2.

Greek symbols

α	volumetric expansion coefficient for a Boussinesq fluid, equation (2)
β	volumetric expansion coefficient for a density-inversion fluid, equation (1)
γ	dimensionless initial temperature (density inversion factor), equation (8)
$\Delta x, \Delta t$	grid spacing and time step using in the numerical calculations
κ	thermal diffusivity
ν	kinematic viscosity
θ	dimensionless temperature $(T - T_m)/(T_m - T_w)$
θ_{BV}	dimensionless temperature used in Fig. 2 $(T - T_c)/(T_h - T_c)$
ρ	density
ψ	dimensionless streamfunction, $u = (1/r)(\partial\psi/\partial z)$, $w = -(1/r)(\partial\psi/\partial r)$.

Subscripts

c	cold wall
h	hot wall
i	initial condition
m	maximum density point
r	reference condition
w	sidewall
I, II, III, IV	transient cool-down stages, I, II, III, IV, respectively, Fig. 7.

were recently conducted by Braga and Viskanta [12] and McDonough and Faghri [13]. In the initial state, motionless and isothermal water at a high temperature $T_i (\geq T_m)$ filled the rectangular cavity. The temperature of one sidewall was abruptly lowered and kept at $T_w = 0°C$, while the opposing wall temperature was maintained at the initial value $T_h = T_i$. Tong and Koster [14] numerically investigated a similar problem using different initial conditions, i.e. $T_i = T_m$. The results illustrated the general influences of density inversion on the transient flow and temperature fields and heat transfer characteristics.

Systematic studies of cool-down (or heat-up) of the entire body of an initially-isothermal liquid with density inversion to a desired temperature have been scarce. Vasseur and Robillard [15] and Robillard and Vasseur [16] numerically investigated the transient natural convection of water in a rectangular cavity, by varying the aspect ratio and the initial water temperature in the range $4°C \leqslant T_i \leqslant 10°C$. Temperatures at all solid boundary walls were abruptly changed to 0°C. Time-dependent evolutions of the subsequent flow and temperature fields were portrayed. The principal finding was that the overall cool-down process could be divided into three distinct transient stages. Due to the density inversion effects in the course of cooling, the transient flow pattern encompassed a single-cell flow, a bi-cellular flow, and finally a newly-developed single-cell flow. These works [15, 16] produced valuable information, however, their results were restricted to the range of relatively small Rayleigh numbers, 2.9×10^3 to 8×10^4. Therefore, the convection effects were not pronounced; consequently, the time-dependent variations of the numerically-acquired Nusselt number did not deviate much from the pure conduction solution. In addition, due to the limited coverage of the relevant parameters, the effects of the Rayleigh number and of the initial temperature (the density inversion factor) on the global cool-down process were not elucidated.

In this study, comprehensive and detailed numerical simulations are carried out to describe the cool-down of a liquid contained in a vertical cylinder through its maximum density temperature. The present calculations cover a much extended range of values of Ra, A and γ, $10^5 \leqslant Ra \leqslant 10^7$, $1.0 \leqslant A \leqslant 10.0$, and $0.0 \leqslant \gamma \leqslant 3.0$. The objective is to gain a thorough basic understanding of the underlying physical phenomenon in the convective cool-down process encompassing the maximum density temperature. The

impetus of this paper is to depict dominant transient flow and temperature fields and the associated cooling characteristics of cool-down. Emphasis will be given to the specific influence of density inversion on the transient cooling process. Special concern will be given to depicting the distinctive transient phases. Scalings will be provided to characterize each transient stage. The effects of the Ra, A, and γ will be scrutinized.

2. MATHEMATICAL FORMULATION AND NUMERICAL SOLUTION

Consider a vertically-mounted cylindrical container, which is completely filled with a liquid, with its maximum density occurring at $T = T_m$. The fluid is initially at rest and isothermal at temperature $T_i (\geqslant T_m)$. At $t = 0$, the whole vertical sidewall is abruptly cooled to temperature T_w ($< T_m$). The horizontal endwalls are thermally insulated. Figure 1 shows a schema of the flow configuration and coordinate system. It is assumed that the fluid is Newtonian and incompressible, and all the fluid properties are constant except for the density in the buoyancy term. The density is assumed to obey a parabolic density–temperature relationship in the vicinity of the maximum density temperature T_m [19]:

$$\rho/\rho_m = 1-\beta(T-T_m)^2. \tag{1}$$

For comparison, the conventional Boussinesq fluid approximation states a linear density–temperature relationship:

$$\rho/\rho_r = 1-\alpha(T-T_r) \tag{2}$$

where ρ_r and T_r indicate reference quantities.

The flow is governed by the time-dependent Navier–Stokes equations, which, in nondimensional form, are expressed as

$$\frac{\partial u}{\partial t}+\frac{1}{r\partial r}(ru^2)+\frac{\partial}{\partial z}(wu) = -\frac{\partial p}{\partial r}+\left(\frac{Pr}{Ra}\right)^{1/2}\left(\nabla^2 u-\frac{u}{r^2}\right) \tag{3}$$

$$\frac{\partial w}{\partial t}+\frac{1}{r\partial r}(ruw)+\frac{\partial}{\partial z}(w^2) = -\frac{\partial p}{\partial z}+\theta^2+\left(\frac{Pr}{Ra}\right)^{1/2}\nabla^2 w \tag{4}$$

$$\frac{\partial \theta}{\partial t}+\frac{1}{r\partial r}(ru\theta)+\frac{\partial}{\partial z}(w\theta) = \left(\frac{1}{RaPr}\right)^{1/2}\nabla^2\theta \tag{5}$$

$$\frac{1\partial(ru)}{r\ \partial r}+\frac{\partial w}{\partial z} = 0 \tag{6}$$

where

$$\nabla^2 = \frac{1}{r\partial r}\frac{\partial}{\partial r}r\frac{\partial}{\partial r}+\frac{\partial^2}{\partial z^2}.$$

Note that, as shown in nomenclature, the Rayleigh number is defined by using the difference between the maximum density and the density at the cold sidewall. This definition of Ra is similar to that of the cold-side Ra adopted by Lankford and Bejan *et al.* [6]. A slightly different form of Ra was selected in refs. [12–13, 15], in which the density difference $\Delta\rho \equiv \rho_m - \bar{\rho}$, $\bar{\rho}$ denoting the density at the mean temperature $(T_i+T_w)/2$, was employed.

In line with the problem description, the initial and boundary conditions are

$$u = w = 0 \quad \text{and} \quad \theta = \gamma, \quad \text{for } t < 0 \tag{7}$$

where

$$\gamma = (T_i - T_m)/(T_m - T_w) \tag{8}$$

and for $t \geqslant 0$

$$u = w = 0 \quad \text{and} \quad \theta = -1 \quad \text{at} \quad r = 1 \tag{9}$$

$$u = \frac{\partial w}{\partial r} = \frac{\partial \theta}{\partial r} = 0, \quad \text{at} \quad r = 0 \tag{10}$$

$$u = w = \frac{\partial \theta}{\partial z} = 0, \quad \text{at} \quad z = 0 \quad \text{and} \quad z = A. \tag{11}$$

Clearly, γ in equation (8) indicates the level of the initial-state temperature T_i, relative to T_m and T_w; γ will be termed the density inversion factor.

The above system of equations was solved numerically by employing a finite-volume procedure based on the SIMPLER algorithm [20]. The governing equations were discretized on a staggered grid. Spatial differencing schemes of second-order accuracy were adopted for the equation terms. A central differencing was used for the diffusion terms, and a recent version of the QUICK scheme [21] was utilized for the nonlinear convective terms. All of the boundary conditions were treated by using second-order differencings. Time integration was accomplished by using an iterative Eulerian implicit method of first-order

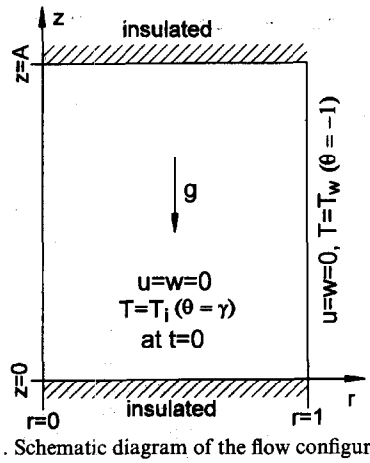

Fig. 1. Schematic diagram of the flow configuration.

accuracy in time. The resulting accuracy of the present method is $O(\Delta t, \Delta x^2)$. Convergence of the solutions was declared at each time step when the maximum relative change between two consecutive iteration levels falls below 10^{-4} for u, w and θ. A parallel checking was performed to ensure that mass continuity in every computational control volume should be satisfied within a relative error 10^{-8}.

Verification of the present numerical model was achieved by repeating a multitude of calculations of the previous results [12–15]. Figure 2 illustrates the reliability and accuracy of the present numerical model. The experiment no. 1 ($T_i = T_h = 8°C$, $T_w = 0°C$, $Pr = 11.82$) of Braga and Viskanta [12] was reproduced and the results at two time instants were compared with their numerical and experimental results. For this test, a grid network of 62×62 nodes was used and the time step, Δt, was 1 s. To resolve thin boundary layers adjacent to the solid walls, grid stretching was implemented. The flow patterns and temperature fields are in general agreement with the numerical results of Braga and Viskanta (see Figs. 2 and 3 in [12]). A small difference is found in the size of the circulating cell in the lower left corner. The present numerical model produced a bigger cell, which is in closer agreement with the visualized flow patterns (see Fig. 4 in [12]). Comparisons were also made of the horizontal temperature profiles at three representative heights (see Fig. 5 in [12]). Additional runs were made with different grids and time steps. For the temperature field at 15 min (at 30 min), the maximum difference between the 62×62 and the 82×82 nodes was 4.9% (10.4%), and the maximum difference between the 62×62 and the 102×102 nodes was 5.8% (15.3%). Slight differences were seen near the border between the two counter-rotating cells across which the temperature varies sharply. In other regions, the differences at 15 min (30 min) were less than 1% (2%).

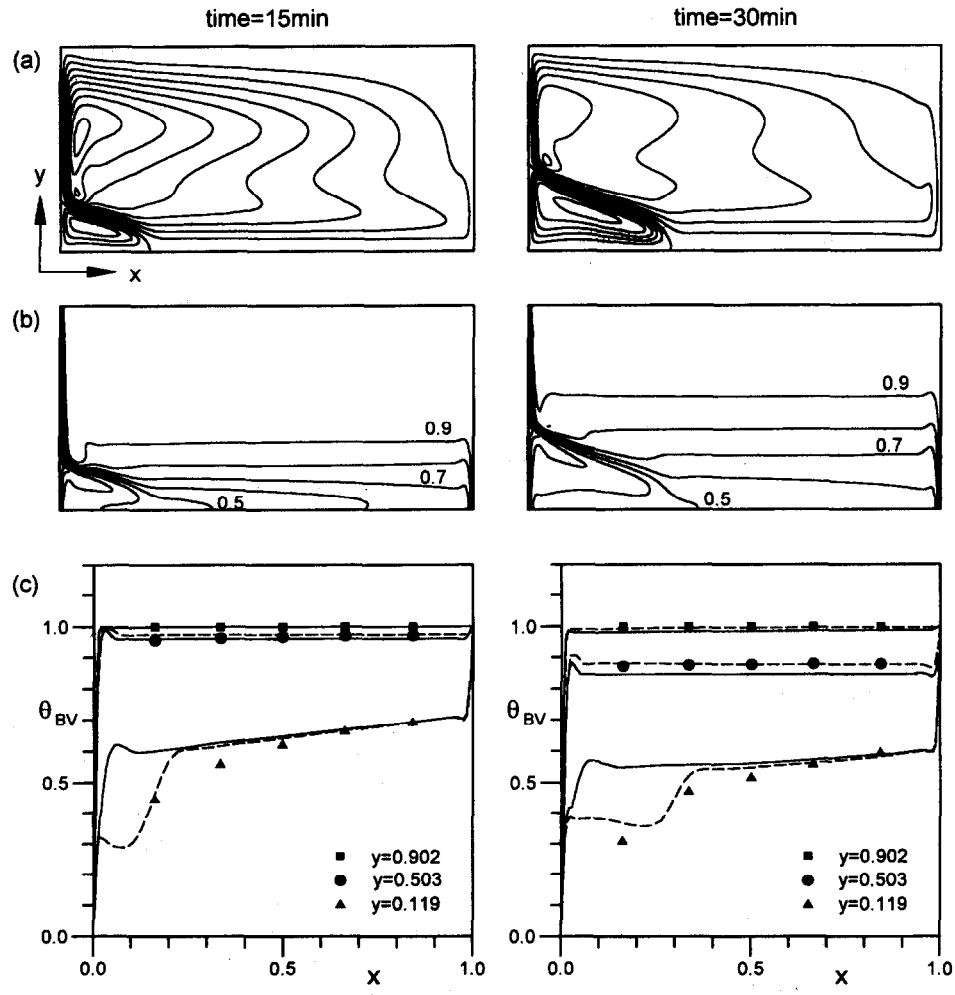

Fig. 2. Results of a verification test of the present numerical method for Experiment no. 1 of Braga and Viskanta [12]. The time instants are 15 min for left column and 30 min for right column. (a) Predicted streamlines, (b) predicted isotherms, (c) horizontal profiles of temperature at three different height. In Fig. 2(c), the solid lines and symbols represent the numerical and experimental results of Braga and Viskanta [12], respectively, and the present numerical results are shown by broken lines.

The solutions were shown to be insensitive to Δt if Δt is small enough to fully resolve the boundary layer formation.

3. RESULTS AND DISCUSSION

Numerical computations were conducted for selected sets of (Ra, A) by varying γ in the range $0 \leqslant \gamma \leqslant 3.0$. The Prandtl number, Pr, was set $Pr = 11.573$ which is the typical value for water near 3.98°C. The computed cases are listed in Table 1. Depending on the values of Ra and A, grid meshes and time step were adjusted, as displayed in Table 1. Grid stretching was implemented such that at least five points were located in the thermal boundary layer.

3.1. *Early-time flow characterization*

It is noted that $Ra/Pr^4 \gg 1$ for all of the present runs. The flow regime in the early stage is of the boundary-layer type [12, 13, 22]. In response to the impulsive change in the sidewall temperature, the thermal boundary layer forms on the sidewall, in which vertical flow is induced by buoyancy force. This layer grows to a thickness of $O(Ra^{-1/4}Pr^{1/2}A^{1/4})$ in time $t \sim O(Pr^{1/2}A^{1/2})$ until the heat conducted out to the sidewall balances that convected in by the vertical currents. Since $Pr > 1$, momentum is diffused into the core outside the thickness of thermal boundary layer. This generates a secondary viscous layer, which is governed by the inertia–viscous balance.

This assertion is valid in depicting the general early-time behavior of cool-down. However, in comparison with the Boussinesq fluid, the buoyancy-induced flow of a fluid with density inversion presents a more complicated picture. For $\gamma > 0$, there exists a buoyancy force reversal inside the thermal boundary layer; the sign of the buoyancy force is positive (upward) in the wall-side of the boundary layer while it is negative (downward) in the core-side [23, 24]. Owing to this character, three flow patterns, depending on the value of γ, can be identified at early times in the thermal boundary layer, which are schematically illustrated in Fig. 3.

When γ is small, the positive buoyancy force prevails in the bulk of the vertical thermal boundary layer. Only in a narrow zone of the layer, the negative buoyancy exists. However, this negative buoyancy is outweighed by viscous shear force, which is locally effective in such a thin area between the dominant upward motion and the solid wall. Consequently, the resulting boundary layer flow is predominantly upward, which is referred to as flow regime I. On the other hand, for large γ, a situation opposite to the cases of small γ develops. The buoyancy force is mostly negative in the vertical thermal boundary layer. The positive buoyancy force is restricted in a very narrow region adjacent to the sidewall. Accordingly, the flow in the vertical thermal boundary layer is predominantly downward, which is referred to as flow regime III. The intermediate pattern, flow regime II, is seen for a moderate value of γ. A flow reversal, associated with the buoyancy force reversal, exists; both the upward and downward motions are present in the vertical thermal boundary layer. This is the case when the magnitudes of positive and negative buoyancy forces are comparable.

Table 1. Computed sets of (Ra, A), and the grid points and time steps used for the calculations

Ra	A	Grid points	Time step, Δt
10^5	1.0	52×52	0.01
10^6	1.0	62×62	0.01
10^7	1.0	72×72	0.01
10^5	2.0	62×72	0.01
10^5	5.0	72×102	0.005
10^5	10.0	82×122	0.005 for $\gamma \leqslant 1.0$ 0.002 for $\gamma > 1.0$

The results of the present runs are summarized in Fig. 3. The essential qualitative character of flow in the early stage of cool-down can be classified into the above-described three categories. The influences of Ra and A in determining the flow regime are generally meager. The qualitative flow characteristics at early times of the cool-down process are determined mainly by a single parameter γ. In this study, only discrete points in the parameter space were covered. Therefore, it posed difficulties in evaluating the exact values of γ for the observed demarcations between two flow regimes. Obviously, flow regimes I and III are observed for small and large values of γ, respectively, and flow regime II occurs only in a narrow range of γ.

3.2. *Description of the overall cool-down process*

The overall cool-down process of flow regime I is similar to that of a Boussinesq fluid with a negative value of α in equation (2) [22]. As the sidewall boundary layer is fully developed, the upwelling currents via the sidewall boundary layer produce a viscous intrusion layer, which propagates in the horizontal direction near the upper endwall. The front of the cold fluid parcels moves downward in the interior core after the horizontal intrusion layer reaches the central axis of the cylinder. Following the front movement, a stable density stratification is established in the interior core. According to the previous scaling argument [2, 22], this process takes a convective time scale, $t \sim O(Ra^{1/4}Pr^{1/2}A^{1/4})$. Afterwards, convective cooling in the interior progresses, and the mean temperature of the interior fluid decreases. This implies a decrease in the effective Rayleigh number, which results in a decrease in cooling rate at the sidewall. The circulations weaken with time, and cool-down in this stage slows down. Finally, the flow undergoes a slow diffusively-controlled approach toward the stationary and isothermal steady state.

Although there are differences in flow structures due to flow reversal in the vertical boundary layer, the

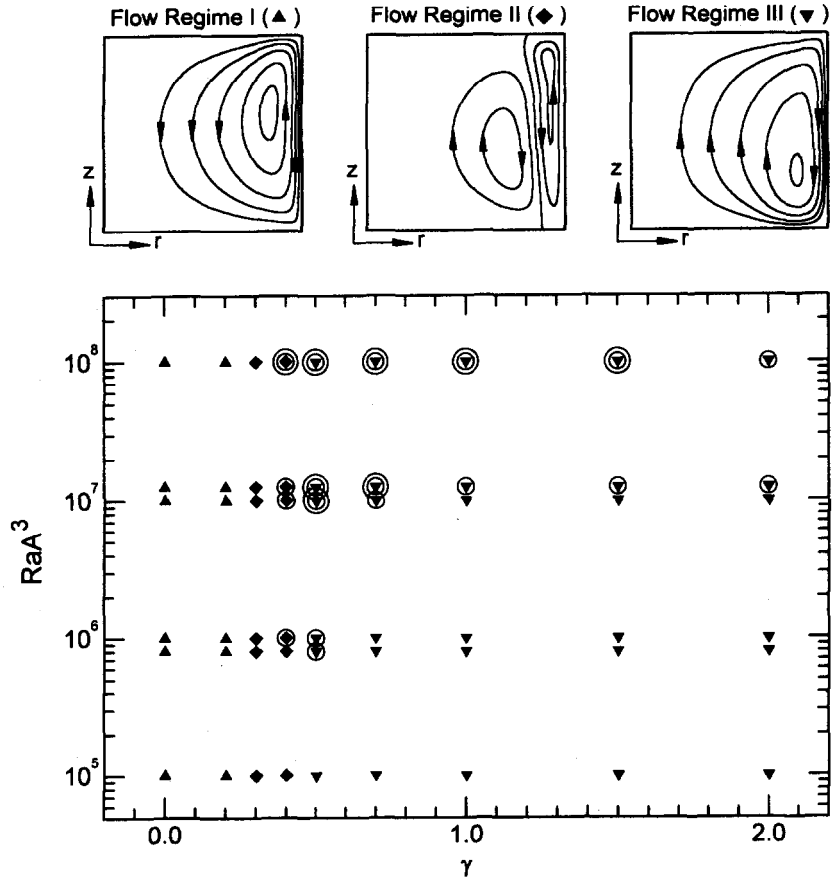

Fig. 3. Computed points in the γ–Ra domain. In the figure, ▲ represents flow regime I; ◆, flow regime II; ▼, flow regime III. Each flow regime is schematically illustrated in the figure. A single circle represents the cases in which a weak secondary boundary layer wave forms. The double circles indicate the cases in which more than three boundary layer waves are developed.

essential features of the overall cool-down of flow regime II (upper horizontal intrusion, downward front movement, and the final cool-down stage) are qualitatively similar to that of flow regime I.

Representative plots showing the transient response of flow regime III are exemplified in Fig. 4, for $Ra = 10^7$, $A = 1.0$, and $\gamma = 1.0$. In Fig. 4(a), the vertical boundary layer forms at early times. The flow in the vertical boundary layer is entirely downward. Accordingly, the full cylinder has the CW (clockwise) circulations only, and the horizontal intrusion is seen in the lower part of the cylinder. It is noticeable in Fig. 4(b) that a CCW (counter-clockwise) circulation cell appears. The evolution of this CCW circulation cell can be explained by the following considerations. The horizontal intrusion delivers cold fluid parcels to the lower part of the cylinder. The maximum density line ($\theta = 0$) moves further toward the interior side. In the lower corner region, θ becomes negative and ρ decreases monotonically toward the sidewall. Consequently, the positive buoyancy force is created in this region. This, in turn, induces upward velocity near the sidewall, which generates an isolated new CCW circulation cell in the lower corner region. The presence of the upward velocity in the lower corner region implies that there exists a separation point in the vicinity of the sidewall across which the boundary layer flow changes its direction.

Here, it is important to describe the roles of the CW and CCW circulations. The CW circulations provide convective cooling in the interior by delivering cold fluid parcels which were cooled at the sidewall. Due to the CW circulations, the front of cold fluid parcels propagates upward in the interior. Following the front, a stable density stratification is established in the interior. With the progress of the core stratification, the CW circulations weaken and they vanish at large times. Heat transfer at the sidewall in the region of the CCW circulation cell (below the separation point) cools the fluid in this isolated region. This causes the isolated CCW circulation cell to grow with time. Since the stable stratification in the interior blocks the horizontal expansion, this CCW circulation cell grows mainly in the vertical direction along the sidewall, as shown in Figs. 4(b–d). This transient character, termed the sidewall boundary layer restructuring, is a phenomenon unique to flow regime III. As the sidewall boundary layer restructuring is fully achieved, a second horizontal intrusion appears in the upper part of the cylinder. As shown in Fig. 4(e, f),

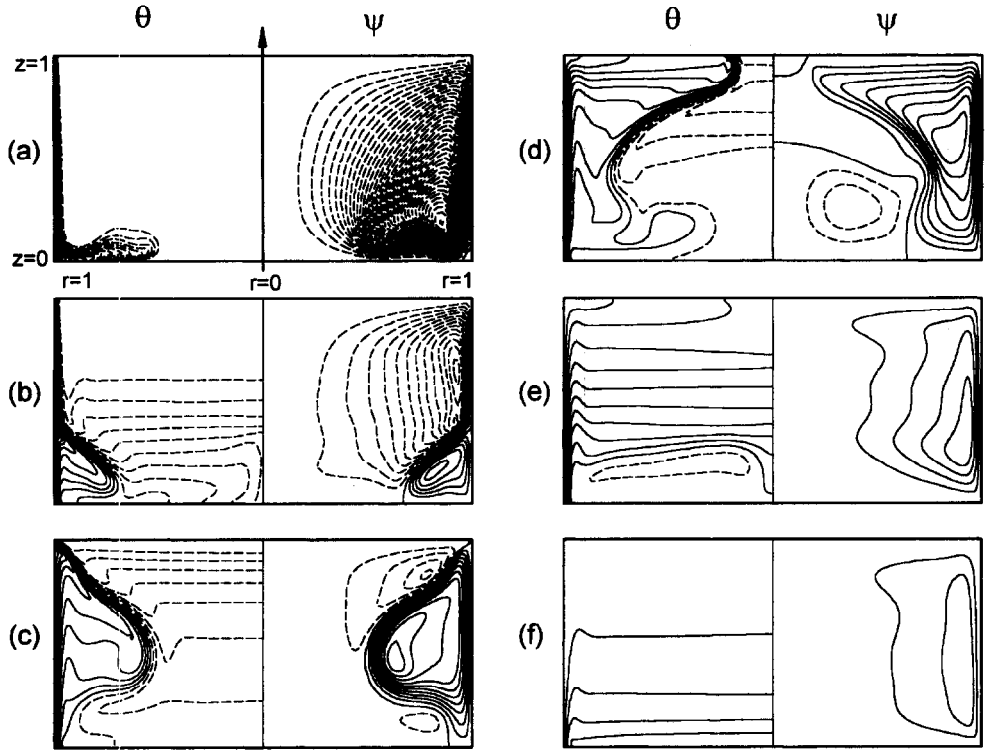

Fig. 4. Sequential plots showing isotherms (left half) and stream functions (right half). $Ra = 10^7$, $A = 1.0$, and $\gamma = 0.0$. The time instants are: (a) $t = 5$; (b) $t = 30$; (c) $t = 90$; (d) $t = 140$; (e) $t = 220$; (f) $t = 400$. The contour increments are $\Delta\psi = 0.0005$ and $\Delta\theta = 0.1$. Isotherms of positive θ, and the contours plots for negative ψ (CW circulation) are shown by broken lines.

the transient process afterwards is akin to that discussed for flow regime I.

The flow restructuring in the cool-down of an enclosed fluid with density inversion was reported by Vasseur and Robillard [15]. Figure 2 of [15] showed the presence of three transient stages, which depicted the results of the specific case for $\gamma = 1.0$ (this belongs to the flow regime III of the present paper). At the beginning of cooling process, a CW circulation cell is induced in the right half cavity. In the next stage, a CCW circulation cell is created from the lower right corner region, and it grows upward to push the original CW circulation cell. However, the transient restructuring in [15] was not restricted in the region adjacent to the sidewall; the newly-developed CCW circulation cell occupies the full lower part of the cavity, spanning horizontally from the interior to the sidewall. As a result, the flow pattern in this stage displays two counter-rotating circulation cells which are vertically stacked. This discrepancy can be attributed to the difference in the thermal boundary condition; the horizontal walls of the cavity considered by Vasseur and Robillard [15] are a perfectly conducting wall of $T = T_w$. Due to the constant-temperature condition at the horizontal walls, the line of the maximum density lied in the horizontal direction. Along this line, the newly-developed CCW circulation could grow in the horizontal direction.

The transient phenomenon similar to the boundary layer restructuring was also explored in unsteady natural convection of a fluid near its density maximum in a sidewall-heated cavity [12–14]. The transient flow patterns for the cases with a large density inversion reveal a pair of counter-rotating circulation cells (see, e.g. Fig. 2). Near the lower corner of the cold wall, a circulation cell is seen which rotates in the opposite direction to the dominant circulation which occupies most of the cavity. It is conspicuous in Fig. 3 of ref. [13] that this corner cell grows upward along the sidewall. Owing to the constraint in their problem setup, this cell stopped growing at a certain vertical level. The full boundary layer restructuring depicted in the present cool-down problem was not discussed explicitly.

3.3. *Development of boundary waves*

Figure 5 shows the results at high Ra ($Ra = 10^7$), with $\gamma = 0.5$, and $A = 1.0$. The general features of boundary layer restructuring process are similar to that in Fig. 4. However, it is visible that wave-like flow patterns form in the boundary layer below the separation point. There exist two centers of the CCW circulations. Following the primary mode, the secondary and higher-mode waves are discernible and they move in the upward direction with time.

These transient flow characteristics are also monitored at a lower Ra with a large aspect ratio. Figure 6 exemplifies the boundary layer restructuring process

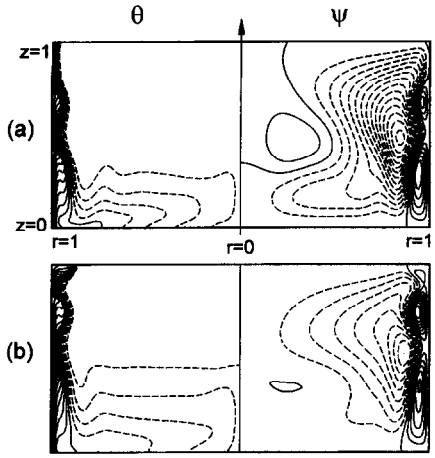

Fig. 5. Same as in Fig. 4, except for $\gamma = 0.5$, $Ra = 10^7$. (a) $t = 25$; (b) $t = 40$. $\Delta\psi = 0.005$ for positive ψ and $\Delta\psi = 0.001$ for negative ψ.

Fig. 6. Same as in Fig. 5, except for $A = 10.0$ and $Ra = 10^5$. (a) $t = 25$; (b) $t = 40$; (c) $t = 55$. $\Delta\psi = 0.005$.

for $Ra = 10^5$, $A = 10.0$, and $\gamma = 0.5$. Initially, a CCW cell appears in the lower corner region and it moves upward. However, the boundary layer below the separation point becomes unstable, thus, it generates subsidiary modes. In Fig. 6(c), three waves travelling along the sidewall are seen. The flow exhibits several CCW cells and CW cells, which are arranged in the vertical direction. After the primary mode of the boundary layer restructuring reaches the upper endwall, the cold parcels propagate downward in the interior core region. The developed waves travel upward and disappear eventually as the front of cold fluid parcels moves downward in the interior core.

The above-described boundary layer waves were previously ascertained in other flow configurations, e.g. natural convection of a Boussinesq fluid in the sidewall-heated cavity [25, 26]. For a very large Ra with $A = O(1)$ [25], or a moderately large Ra with a large A [26], boundary layer waves were reported to develop. One assertion is that these waves may be responsible for bringing permanent unsteadiness and, thus, providing origins of turbulence.

The present results concerning the existence of boundary layer waves are also summarized in Fig. 3. It is obvious that the boundary layer waves are captured when Ra and A are large, namely, the Rayleigh number based on the vertical height of the cylinder, Ra_H ($\equiv RaA^3$), is sufficiently large. At a relatively small Ra_H (indicated with a single circle in Fig. 3), only a weak secondary wave forms, but it soon decays due to the pronounced viscous and thermal diffusions. At a larger Ra_H, the generation of boundary layer waves becomes more active, and several succeeding modes are created, although they disappear eventually with the progress of cool-down. Here, it is worth pointing out that, in the present cool-down problems, the boundary layer waves are developed at a much smaller Ra_H than for a Boussinesq fluid. In sidewall-heated cavity with $A = 1$, they are seen for $Ra \sim 10^9$ [25]. In particular, as shown in Fig. 3, the boundary layer waves are developed at a much smaller Ra_H for moderate values of γ (e.g. $\gamma = 0.5$) than for small or large values of γ. A plausible explanation can be made. The flow reversal in the boundary layer due to density inversion is most conspicuous near the border of flow regimes II and III. The boundary layer is prone to instability in the presence of flow reversal. The velocity shear due to the flow reversal creates an environment for the boundary layer to be unstable so as to generate boundary layer waves. Consequently, owing to the density inversion, the boundary layer instability is seen to occur at a much smaller Ra_H than for a Boussinesq fluid.

3.4. *Transient phases and cool-down time scales*

Figure 7 depicts the temporal variation of the Nusselt number at the sidewall for the case of $Ra = 10^7$, $A = 1.0$, and $\gamma = 1.0$. The Nusselt number, Nu, is defined as

$$Nu = -\frac{1}{A}\int_0^A \left.\frac{\partial\theta}{\partial r}\right|_{r=1} dz. \tag{12}$$

Figure 7 suggests that the full cool-down process can be divided into four distinguishable transient phases. The first, phase I, represents the formation of the sidewall boundary layer. Nu decreases very rapidly with the growth of thermal boundary layer, although the overall value of Nu is very large. In phase II, Nu decreases at a reduced rate. Phase II is associated with

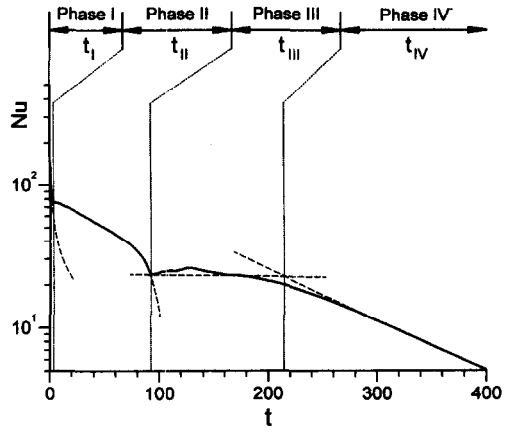

Fig. 7. Phases in the evolution of the Nusselt number. $Ra = 10^7$, $A = 1.0$, and $\gamma = 1.0$.

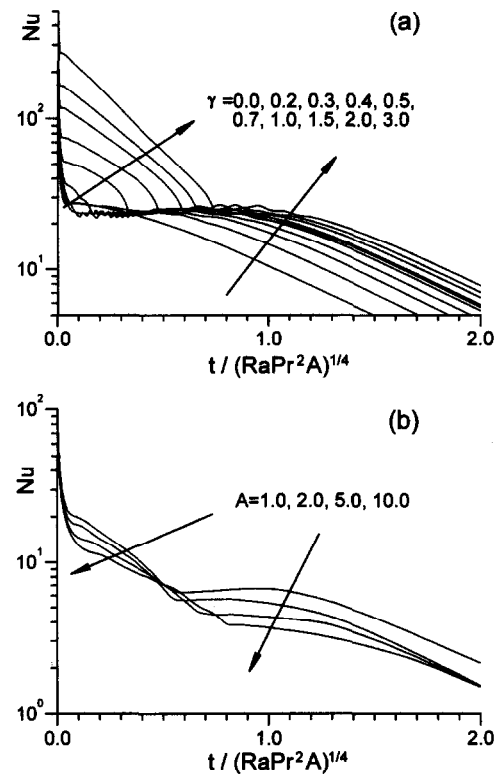

Fig. 8. Effects of γ and A on the evolution of Nu. (a) $Ra = 10^7$ and $A = 1.0$; (b) $Ra = 10^5$, $\gamma = 1.0$.

the afore-mentioned sidewall boundary layer restructuring. The thermal boundary layer thickness above the separation point is smaller than that below the separation point. Consequently, the heat transfer rate decreases with the advance of boundary layer restructuring. Phase III corresponds to the transient stage, in which the upper horizontal intrusion and the downward propagation of the cold fluid parcels with $\theta < 0$ take place. In this phase, temporal variations of Nu are very small, since the structure of the thermal boundary layer remains virtually unchanged. In the final phase IV, Nu decreases slowly with time, which is closely related to the afore-mentioned decrease in the effective Rayleigh number.

The effect of γ on the temporal behavior of Nu is illustrated in Fig. 8(a). It is seen that phase II, related to the boundary layer restructuring, exists only for $\gamma \geqslant 0.5$, while phases I, III and IV are discernible for all the cases. The time duration for phase II increases with γ. The general transient behavior in phases I, III and IV is similar. The temporal oscillations which are seen in phase III for $\gamma \geqslant 0.4$ indicate the influences of boundary layer waves. The oscillations of small frequencies are more pronounced for $\gamma = 0.4$ and 0.5. These are in line with the regime diagram of Fig. 3. The effect of A on time-dependent heat transfer characteristics is demonstrated in Fig. 8(b). It is notable that the qualitative features of overall transient heat transfer become similar if the abscissa is expressed as $t/(RaPr^2A)^{1/4}$. In particular, the effect of A is inconspicuous in phase IV.

Finally, discussions will be focused on the issue of the relevant time scales in cool-down. The characteristic cool-down time scales can be assessed by examining the time durations of the afore-mentioned transient phases. The transition between two successive phases is judged by means of the graphical analyses of the time-dependent Nu curves as shown in Fig. 7. The characteristic curves of four phases are acquired by fitting the numerical data, and the transition is identified by searching for the intersection point of the curves of two successive phases. The final adjustment process at large times in phase IV becomes diffusive in nature, and it takes place over a long time span. Thus, the time duration for phase IV is estimated up to the time at which the mean fluid temperature becomes -0.9. Admittedly, a certain amount of arbitrariness is involved in the present classifications of relevant phases. The main effort is to provide an overall descriptive picture of qualitative essentials of the global cool-down process.

Based on the above method, the time scales of the four transient phases were calculated, which are summarized in Fig. 9. It is clear that t_I increases with γ, and t_I reaches a maximum around $\gamma = 0.4$. For large values of γ, t_I decreases in proportion to $1/\gamma$. This is due to the fact that the heat transfer rate of flow regime II is smaller than those of flow regimes I and III. Note that the boundary layer thickness in the former case is larger than that of latter cases. Consequently, for flow regime II, it takes more time for the sidewall boundary layer to grow to its full thickness. However, a precise estimation of t_I is immaterial; the overall magnitude of t_I is much smaller than the other time scales.

The estimated values of t_{II} are plotted in Fig. 9(b). It is immediately clear that t_{II} increases with γ; the effects of Ra and A on t_{II}, scaled by $Ra^{1/4}A^{1/3}$, are minor. Data analysis of the numerical results leads to a correlation

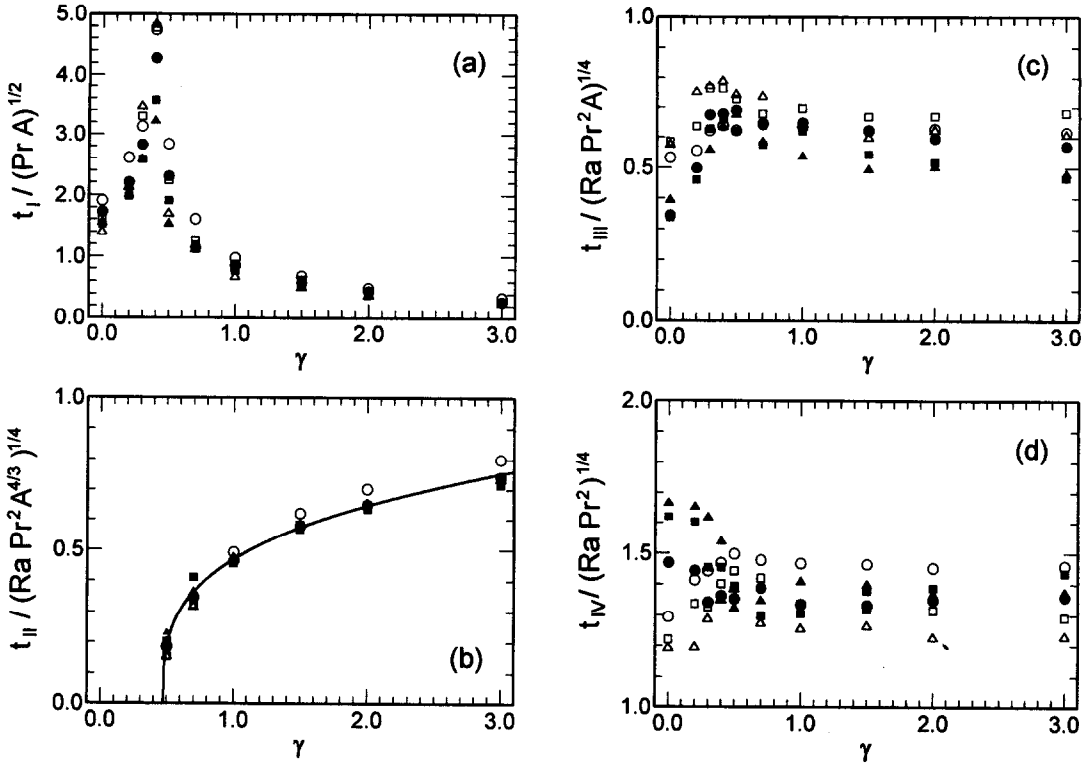

Fig. 9. Scaled time durations for each phase described in Fig. 7. (a) t_I; (b) t_{II}; (c) t_{III}; (d) t_{IV}. ○, $Ra = 10^5$, $A = 1.0$; □, $Ra = 10^6$, $A = 1.0$; △, $Ra = 10^7$, $A = 1.0$; ●, $Ra = 10^5$, $A = 2.0$; ■, $Ra = 10^5$, $A = 5.0$; ▲, $Ra = 10^5$, $A = 10.0$. In Fig. 9(b), the line indicates the values of t_{II} estimated by equation (13).

$$t_{II}/(Ra^{1/4}Pr^{1/2}A^{1/3}) = 0.5686(\gamma - 0.4771)^{0.2996} \quad (13)$$

which is shown in the solid-line curve in Fig. 9(b).

Figures 9(c) and (d) display t_{III} and t_{IV}. The impact of γ on t_{III} and t_{IV} is noticeable only for small values of γ. In particular, t_{III} and t_{IV} are nearly independent of γ for large values of γ. In addition, t_{III} and t_{IV}, scaled by $(RaA)^{1/4}$ and $Ra^{1/4}$, respectively, exhibit only minor dependency on Ra and A. This provides an order-of-magnitude estimation for t_{III} and t_{IV}. The independence of t_{III} and t_{IV} of γ can be explained by the following physical argument. It can be deduced from Fig. 4 that the mean temperature falls below 0 in phase III. This implies that the explicit effect of the density inversion decays in this phase. It is worth recalling that the density inversion effects are represented by the parameter γ. The present Ra is based on the difference between the maximum density and the density at the cold sidewall. Therefore, Ra in the present study is decoupled from the direct effect of density inversion.

By using the definitions of γ and Ra in the present formulation, the effect of γ turns up mostly in the early stages of cool-down when the density inversion is a principal dynamic element. The effect of A becomes insignificant with the progress of cool-down. The parameter Ra becomes the dominant controlling factor in the intermediate- and large-time adjustment processes when the density inversion effect has subsided.

4. CONCLUSION

The early-time behavior of the boundary-layer flows is controlled largely by the density inversion factor γ. Evolutions of the global fields of velocity and temperature are characterized by Ra and A when γ is very small, and the general features are similar to those of the conventional Boussinesq fluid. The flow reversal in the thermal boundary layer is possible for intermediate values of γ. For large γ, a single cell flow structure is initially developed by the downward flow in the boundary layer. Then, the subsequent boundary layer restructuring is accomplished due to density inversion, which describes the upward growth of the newly-developed counter-rotating circulation cell. The horizontal intrusion and downward convective filling of cold fluid parcels are seen to follow. Afterwards, slow convective cooling of the fluid is achieved at large times.

The results of the present computations disclose the presence of boundary layer waves travelling along the sidewall. These waves emerge for large Ra_H, but they are developed at a much smaller Ra_H for moderate values of γ than for a Boussinesq fluid. Together with the boundary layer restructuring, these are reflective of the pronounced effects of density inversion in the transient cool-down process.

The temporal variations of Nu disclose the presence

of four distinct phases, which is in line with the description of transient flow and temperature fields. The time durations of the early phases are strongly affected by the strength of density-inversion. The overall times pertinent to the global adjustment process are shown to scale with $Ra^{1/4}$.

Acknowledgements—The authors are grateful to Dr S. Mizutani and Mr T. Ishiguro of Kirin Brewery Co. Ltd, Japan, for their suggestion for this study. The calculations were carried out at the supercomputer center of The Institute of Space and Astronautical Science (ISAS). This work was supported in part by a grant from the Center of Excellence (COE) Program of the Ministry of Education, Science, Sports and Culture, Japan.

REFERENCES

1. Ostrach, S., Natural convection in enclosures. *Journal of Heat Transfer*, 1988, **110,** 1175–1190.
2. Hyun, J. M., Unsteady buoyant convection in an enclosure. *Advances in Heat Transfer*, 1994, **24,** 277–320.
3. Gebhart, B. and Mollendorf, J. C., Buoyancy-induced flows in water under conditions in which density extremums may arise. *Journal of Fluid Mechanics*, 1978, **89,** 673–707.
4. Vasseur, P., Robillard, L. and Chandra Shekar, B., Natural convection heat transfer of water within a horizontal annulus with density inversion effects. *Journal of Heat Transfer*, 1983, **105,** 117–123.
5. Inaba, H. and Fukuda, T., An experimental study of natural convection in an inclined rectangular cavity filled with at its density extremum. *Journal of Heat Transfer*, 1984, **160,** 109–115.
6. Lankford, K. E. and Bejan, A., Natural convection in a vertical enclosure filled with water near 4°C. *Journal of Heat Transfer*, 1986, **108,** 755–763.
7. Lin, D. S. and Nansteel, M. W., Natural convection heat transfer in a square enclosure containing water near its density maximum. *International Journal of Heat and Mass Transfer*, 1987, **30,** 2319–2328.
8. Lin, D. S. and Nansteel, M. W., Natural convection in a vertical annulus containing water near the density maximum. *Journal of Heat Transfer*, 1987, **109,** 899–905.
9. Ho, C. J. and Lin, Y. H., Natural convection heat transfer of cold water within an eccentric horizontal cylindrical annulus. *Journal of Heat Transfer*, 1988, **110,** 894–900.
10. Ho, C. J. and Lin, Y. H., Natural convection of cold water in a vertical annulus with constant heat flux on the inner wall. *Journal of Heat Transfer*, 1990, **112,** 117–123.
11. Robillard, L. and Vasseur, P., Convective response of a mass of water near 4°C to a constant cooling rate applied on its boundaries. *Journal of Fluid Mechanics*, 1982, **118,** 123–141.
12. Braga, S. L. and Viskanta, R., Transient natural convection of water near its density extremum in a rectangular cavity. *International Journal of Heat and Mass Transfer*, 1992, **35,** 861–875.
13. McDonough, M. W. and Faghri, A., Experimental and numerical analyses of the natural convection of water through its density maximum in a rectangular enclosure. *International Journal of Heat and Mass Transfer*, 1994, **37,** 783–801.
14. Tong, W. and Koster, J. N., Density inversion effect on transient natural convection in a rectangular enclosure. *International Journal of Heat and Mass Transfer*, 1994, **37,** 927–938.
15. Vasseur, P. and Robillard, L., Transient natural convection heat transfer in a mass of water cooled through 4°C. *International Journal of Heat and Mass Transfer*, 1980, **23,** 1195–1205.
16. Robillard, L. and Vasseur, P., Transient natural convection heat transfer of water with maximum density effect and supercooling. *Journal of Heat Transfer*, 1981, **103,** 528–534.
17. Yamada, M., Fukusako, S. and Eman-Bellah, M., Melting characteristics of an ice layer immersed in immiscible liquid. *Proceedings of the National Heat Transfer Symposium*, Niigata, Japan, May 1996, pp. 71–72.
18. Yamada, M., Fukusako, S., Takahashi, T. and Yamamoto, H., Onset of free convection and heat transfer characteristics within a horizontal layer of saline water. *Proceedings of the National Heat Transfer Symposium*, Niigata, Japan, May 1996, pp. 379–380 (in Japanese).
19. Debler, W. R., On the analogy between thermal and rotational hydrodynamic stability. *Journal of Fluid Mechanics*, 1966, **24,** 165–176.
20. Patankar, S. V., *Numerical Heat Transfer and Fluid Flow*. McGraw-Hill, New York, 1980.
21. Hayase, T., Humphery, J. A. C. and Grief, R., A consistently formulated QUICK scheme for fast and stable convergence using finite-volume iterative calculation procedures. *Journal of Computational Physics*, 1992, **98,** 108–118.
22. Patterson, J. C. and Imberger, J., Unsteady natural convection in a rectangular cavity. *Journal of Fluid Mechanics*, 1980, **100,** 65–86.
23. El-Henawy, I., Gebhart, B., Hassard, B., Kazarinoff, N. D. and Mollendorf, J. C., Numerically computed multiple steady states of vertical buoyancy-induced flows in cold pure water. *Journal of Fluid Mechanics*, 1982, **122,** 235–250.
24. Hwang, Y., Kazarinoff, N. D. and Mollendorf, J. C., Hydrodynamic stability of multiple steady-states of vertical buoyancy-induced flows in cold pure water. *International Journal of Heat and Mass Transfer*, 1993, **36,** 423–435.
25. Paolucci, S. and Chenoweth, D. R., Transition to chaos in a differentially heated vertical cavity. *Journal of Fluid Mechanics*, 1989, **201,** 370–410.
26. Le Quéré, P., Transition to unsteady natural convection in a tall water-filled cavity. *Physics of Fluids*, 1990, **A2,** 503–514.